Influence of different conjugation methods for activating antibodies on polymeric nanoparticles

Effects for polyclonal expansion of human CD8+ T cells

Weller, Sven; Li, Xin; Petersen, Lars R.; Kempen, Paul; Clergeaud, Gael; Andresen, Thomas L.

Published in:
International Immunopharmacology

Link to article, DOI:
10.1016/j.intimp.2024.111643

Publication date:
2024

Document Version
Publisher's PDF, also known as Version of record

International Immunopharmacology 129 (2024) 111643

Contents lists available at ScienceDirect

International Immunopharmacology

journal homepage: www.elsevier.com/locate/intimp

Influence of different conjugation methods for activating antibodies on polymeric nanoparticles: Effects for polyclonal expansion of human CD8+ T cells

Sven Weller [a,*], Xin Li [a], Lars R. Petersen [a], Paul Kempen [a,b], Gael Clergeaud [a], Thomas L. Andresen [a]

[a] Department of Health Technology, Technical University of Denmark, Kongens Lyngby, Denmark
[b] DTU Nanolab, Technical University of Denmark, Kongens Lyngby, Denmark

ARTICLE INFO

Keywords:
Artificial antigen presenting cell
Antibody presentation
Nanoparticle surface engineering
Immunotherapy
Particle – cell interaction

ABSTRACT

Particle-based systems have become a state-of-the-art method for *in vitro* expanding cytotoxic T cells by tailoring their surface with activating molecules. However, commonly used methods utilize facile carbodiimide chemistry leading to uncontrolled orientation of the immobilized antibodies on the particle surface that can lead to poor binding to target cells. To address this, selective coupling strategies utilizing regioselective chemical groups such as disulfide bridges offer a simple approach. In this work we present a set of methods to investigate the effect of polymeric nanoparticles, conjugated with either regioselective- or randomly-immobilized antiCD3 and antiCD28 antibodies, on the activation potential, expansion and expression of activation markers in T cells. We show that nanoparticles with well-oriented monovalent antibodies conjugated via maleimide require fewer ligands on the surface to efficiently expand T cells compared to bivalent antibodies randomly-immobilized via carbodiimide conjugation. Analysis of the T cell expression markers reveal that the T cell phenotype can be fine-tuned by adjusting the surface density of well-oriented antibodies, while randomly immobilized antibodies showed no differences despite their ligand density. Both conjugation techniques induced cytotoxic T cells, evidenced by analyzing their Granzyme B secretion. Furthermore, antibody orientation affects the immunological synapse and T cell activation by changing the calcium influx profile upon activation. Nanoparticles with well-oriented antibodies showed lower calcium influx compared to their bivalent randomly-immobilized counterparts. These results highlight the importance of controlling the antibody density and orientation on the nanoparticle surface via controlled coupling chemistries, helping to develop improved particle-based expansion protocols to enhance T cell therapies.

1. Introduction

Immunotherapy with *ex vivo* expanded polyclonal T cells has shown potential for treating cancer and virus-dependent immune diseases.[1,2] This therapeutic modality relies on the isolation of lymphocytes from the patient, expansion or modification *ex vivo,* and reinfusion into the patient. T cell expansion requires sufficient stimulation of the T cell receptor (TCR) via peptide-MHC interaction (Signal 1), and further supply of survival signals such as co-stimulation via CD28 (Signal 2) and survival signals provided by cytokines (Signal 3). Optimal expansion protocols not only rely on achieving high numbers of lymphocytes, but also T cells having the ideal phenotypic characteristics. While early phenotypes include properties such as high proliferative potential and antigen independence, late phenotypes get more specialized towards a specific antigen but lose their high proliferative capacity.[3,4] In a therapeutic scenario of adoptive T cell transfer the T cell phenotype impacts the success of the treatment. The ideal T cell product should therefore have strong antigen dependence, high proliferative capacity and a non-exhausted phenotype, which in many studies has been shown to correlate with memory stem cell or central memory T cell phenotypes.[5–7] It is therefore important to develop controlled T cell stimulation methods during ex-vivo engineering of the T cells and bead based stimulations play a central role in current protocols.

Approaches to expand T cells utilize complex co-culture methods

* Corresponding author.
E-mail address: svewel@dtu.dk (S. Weller).

https://doi.org/10.1016/j.intimp.2024.111643
Received 5 January 2024; Received in revised form 31 January 2024; Accepted 31 January 2024
Available online 9 February 2024

with antigen-presenting cells (APCs), hampering the full therapeutic potential of these approaches due to the need for another patient-derived cell.[8] Artificial antigen-presenting cells (aAPCs), either cellular or acellular, have been developed to overcome these limitations and have already shown success in the clinical setup.[9–11] Acellular approaches have gained great attraction due to their easy-to-handle culture conditions and versatility to modify the particle-based systems. In that context, strategies utilizing different materials have been evaluated to improve the potential of aAPCs, including liposomes[12], peptide-based elongated worms[13], inorganic materials such as silica Janus particles[14] or polymer-based systems[15]. Among these, researchers have shown how the size and shape of these particle systems can modulate the cell expansion profiles, mainly due to their increased surface area available for T cell synapsis.[16–19] More importantly, the particle-to-cell ratio and density of signals 1 & 2 per particle are also known parameters to play a key role in T cell activation, showing a high dependence on the amount of antibody immobilized on the surface of the particles.[20,21] To design robust aAPCs, exact knowledge about the antibody/ligand orientation is a key factor to understand and predict T cell activation profiles and phenotypes for later use in clinical setups.

The synthesis of T cell activating particles require the covalent binding of antiCD3/pMHC and antiCD28 antibodies on the surface. The most commonly used strategies are carbodiimide chemistries such as EDC, EDC/NHS and TFP-esters. Carbodiimide chemistry relies on either reactive amine from lysine or carboxyl groups from aspartic/glutamic acid residues, respectively, from which amine-based couplings are more common.[22–24] Due to the biochemical nature of antibodies with a wide distribution of reactive amines, this coupling chemistry is poorly controllable, thus yielding different antibody orientations on the nanoparticle surface. Some of these orientations have been described in the

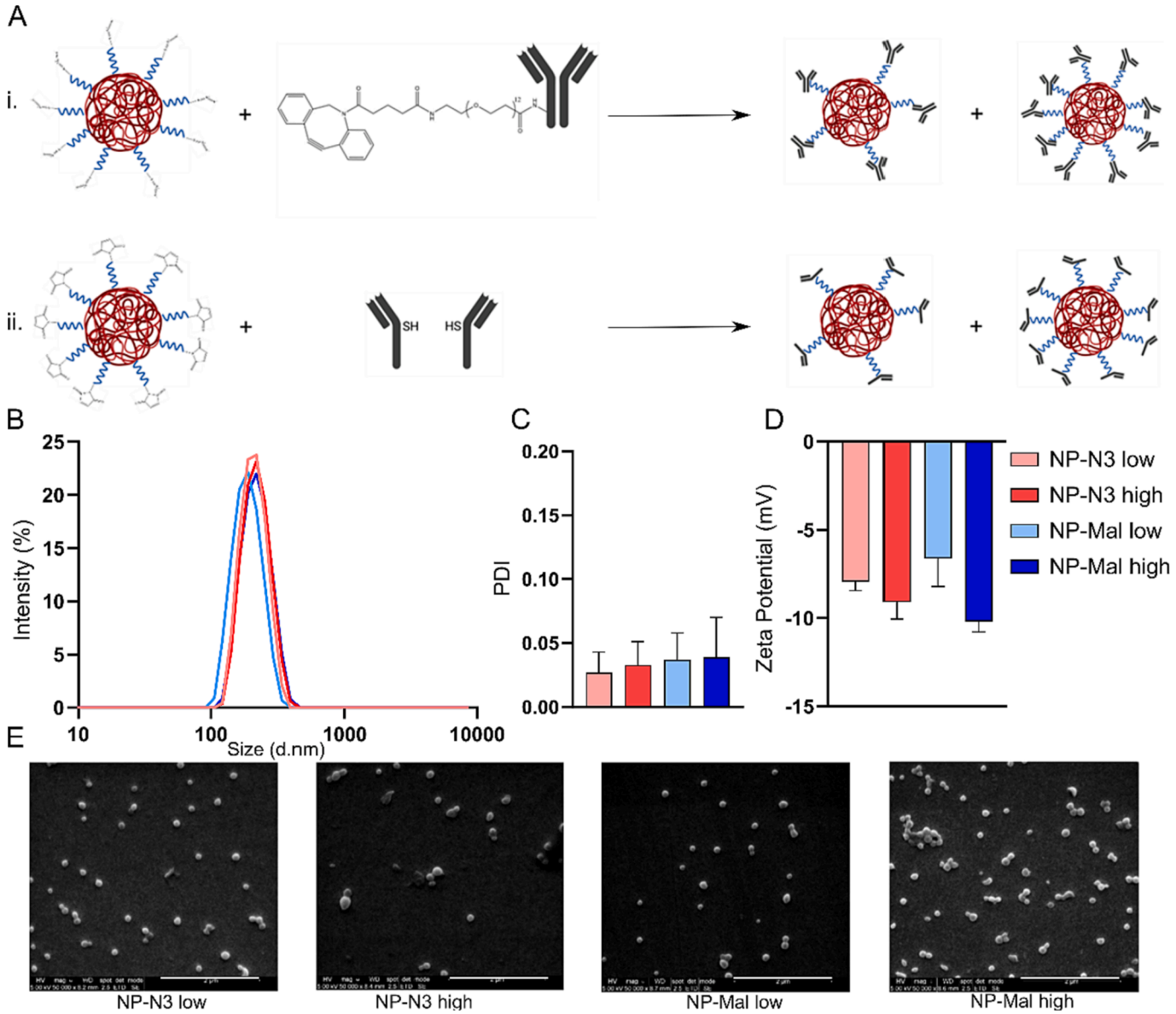

Fig. 1. Design and physicochemical properties of the different nanoparticles. (A) graphical illustration of the synthesis of aAPCs and antibody coupling methods. In all particles, the core consists of coiled PLGA polymers with blue PEG reaching the hydrophilic environment. (i) Particles are end-group functionalized with Azide groups, that are reacting with DBCO-modified full antibodies. (ii) Maleimide functionalized particles, reacting with reduced half-antibodies. Both coupling strategies are carried out at low (1 %) and high (5 %) surface coverage of functionalizable groups. (C) Dynamic light scattering analysis showing the size distribution, (D) Polydispersity evaluation and (E) zeta potential measurements of the aAPCs with different surface chemistries. All three represent mean ± SD (n = 3). (F) Surface electron microscopy images of the different nanoparticles. Scale bars represent 2 μm. (For interpretation of the references to colour in this figure legend, the reader is referred to the web version of this article.)

literature as *tail-on*, *head-on*, *side-on* and *flat-on*, depending on their arrangement,[25] leading to antigen-binding sites being buried towards the nanoparticle surface. An elegant way to overcome this is using site-specific bioconjugation approaches utilizing the sugar chains[26], C-terminal conjugations[27], using intermediate proteins[28], capturing the nucleotide-binding site[29], or opening disulfide bonds[30]. Due to the controlled opening of the hinge region, reactive sulfhydryl's can be created and reacted via Michael-addition to maleimide groups, allowing a more controlled immobilization with good orientation. Matic et al. have demonstrated the importance of well-oriented antibodies for activation of CD4+ T cells using antiCD3 nanoarrays on coated plastics.[21] This highlights the importance of controlling the antibody orientation and density to create systems that allow improved accessibility to receptor-binding sites and ultimately fine-tuning of T cell responses.

In this work, we present a set of methods to evaluate the impact of antibody orientation, valence and density on particle-based systems for polyclonal CD8+ T cell activation and expansion utilizing two different coupling chemistries. We were able to decipher the differences between random and well-oriented coupling strategies, by utilizing a simple workflow including primary human T cells. More precisely, aAPCs with well-oriented antibodies required a lower ligand density to expand T cells and further allowed fine-tuning of the final phenotype. This work highlights the importance to carefully design nanoparticles as efficient aACPs and presents a set of methods to evaluate their performance to activate and expand T cells.

2. Results and discussion

2.1. Synthesis of monodisperse polymeric artificial antigen presenting cells with precise antibody density

To evaluate the impact of antibody orientation, valence, and density of antibodies on the surface of T cell activating aAPCs, two different bioconjugation strategies were chosen, each aiming for two ligand surface densities on a poly(lactic-co-glycolic acid) (PLGA) model system (low, 1 wt%; high, 5 wt%) (Fig. 1A). Studies have demonstrated that unmodified PLGA nanoparticles exhibit notable stability over a duration of 240 h [31].The first coupling technique (i), consists of a random immobilization approach, based on the heterovalent linker TFP-PEG_{12}-DBCO. The tetrafluorophenyl-ester is more resistant towards hydrolysis [32], but targets the same reactive group as conventional EDC/NHS-chemistry, resulting in a carbodiimide bond between the free amine on the surface of the protein and the linker. The DBCO-modified anti-CD3 and anti-CD28 antibodies were coupled in a 1:1 ratio to the surface using copper-free, strained promoted azide-alkyne cycloaddition click chemistry, with free azides exposed on polyethylene-glycol (PEG) chains of the nanoparticle (named NP-N3). Conjugating antibodies via amine bioconjugation onto PLGA nanoparticles may result in a random orientation, potentially hindering the ability to achieve a desired orientation and affecting the binding efficiency of the antibodies [33]. The second conjugation strategy (ii), relies on the cleavage of the antibodies hinge-region or heavy and light chain by selectively reducing the disulfide bridges with Tris-(2-carboxyethyl)-phosphine, thus exposing reactive thiols that are linked via Michael-addition to maleimide groups presented by PEG chains on the surface of the nanoparticle (named NP-Mal). This allows a controlled way of immobilizing both the anti-CD3 and anti-CD28 half-antibodies, but only exposes a monovalent antigen-binding moiety per ligand. In addition, PEG chains were used as spacers for conjugation exploiting their antifouling properties to avoid unspecific antibody adsorption. Studies have indicated that thiol-maleimide conjugation offers a method to regulate the orientation of antibodies on the surfaces of nanocarriers, thereby influencing their targeting properties [34]. After synthesis and bioconjugation of the nanoparticles, the size was analyzed by dynamic light scattering (DLS) showing a narrow size distribution ranging from 185 nm to 230 nm average sizes (Fig. 1B). In addition, all particles had low polydispersity index (PDI < 0.05) indicating homogeneous monodisperse size populations (Fig. 1C). These characteristics are ideal for nanoparticle interaction with the CD3ε on the T cells surface, which forms islands with a width ranging from 40 nm to 300 nm[35]. Zeta Potential measurements indicated a slightly negative surface charge (−10 mV to −7 mV) of the nanoparticles (Fig. 1D), which will lead to light repulsive effects between the aAPC and the T cell membrane, allowing to investigate more closely the effect of the aAPC ligand orientation by eliminating charge interactions.[36,37] Moreover, decreased surface charge can be observed between low and high antibody surface densities, which can be explained by the isoelectric point of the antibodies between 6.6 and 7.2 exposing the negatively charged protein (Fig. 1D)[38]. As per our current understanding, no study has demonstrated any adverse effects of the selected conjugation methods on the colloidal stability of PLGA nanoparticles, thus establishing this study as a representative model.Visualization using scanning electron microscopy (SEM) confirmed the size homogeneity of the nanoparticles as observed by the low PDI values and depicts the spherical shape of the particles after bioconjugation (Fig. 1F).

Studies have shown that the ratio and density of signal 1 and 2 is influencing the expansion rate of T cells, and consequently a key parameter for the design of aAPCs.[39,40] The assessment aimed to verify the attachment of antibodies to the surface of nanoparticles. Instead of employing conventional protein content measurement methods like BCA or Bradford assays, we opted for a different approach. Specifically, we labeled the antibodies, aCD3 and aCD28, with distinct fluorescent markers using the Lightning Link conjugation kit. This allowed for the quantification of each individual antibody. The results of the assay indicated that both types of nanoparticles had comparable amounts of antibodies on their surfaces concerning the occupancy of reactive binding sites, as indicated in Table 1. Notably, nanoparticles with a high surface coverage (5 % reactive groups) exhibited approximately five times more antibody molecules per milligram of particles compared to those with low surface coverage (1 % reactive groups). Interestingly, maleimide nanoparticles bound slightly more antibody molecules than azide nanoparticles. One possible explanation for this difference could be a more efficient coupling reaction, likely attributed to the increased reactivity of the thiols found in reduced antibodies compared to the DBCO moieties on full antibodies. It is noteworthy that the ratio of aCD3 to aCD28 antibodies on all particles fell within a similar range, ranging between 1:1.1 and 1:1.5. This consistency enables a direct comparison between both conjugation methods, given that the antibody ratio remained relatively stable. In conclusion, both nanoparticle systems demonstrated similar physicochemical characteristics, with comparable quantities of antibodies immobilized on their surfaces. Nevertheless, there were variations in the orientation of the antibodies on the particles, presumably due to the specific conjugation methods employed. Owing to the potential impact of attached fluorophores on the antibodies, the particles utilized in the subsequent experiments did not feature fluorophore-conjugated antibodies.

Table 1
Maleimide and Azide particle show similar amounts of Antibody immobilized. Both systems show a percentual increase with higher amounts of reactive surface groups.

	NP-N_3 low	NP-N_3 high	NP-Mal low	NP-Mal high
anti-CD3 (pmol/mg particle)	6.21 ± 1.42	27.96 ± 0.21	8.24 ± 0.98	31.36 ± 0.29
anti-CD28 (pmol/mg particle)	8.00 ± 0.05	42.62 ± 0.14	9.75 ± 0.67	44.63 ± 5.63

2.2. Ca^{2+} sensing provides insight into the binding behavior of the NPs to T cells

Calcium sensing is a well-known tool in order to study T cell activation patterns.[41–43] Ca^{2+} is an important signaling molecule relevant in the activation and proliferation process of lymphocytes[44]. Upon TCR engagement, T cells release intracellular Ca^{2+} from the endoplasmatic reticulum to the cytosol [45], followed by a constant influx of Ca^{2+}, giving distinct Ca^{2+} patterns depending on binding strength and duration that ends with the breakup of the synapsis. Thus, investigating the calcium influx behavior upon stimulation with aAPCs using different coupling chemistries can provide insight into the overall affinity of the system. Here, freshly naïve T cells were isolated, stained with the fluorescent calcium indicator Fluo-4AM and afterwards incubated with aAPCs at a final concentration of 200 μg/ml. To study the differences of binding upon NP interactions, different parameters were analyzed as depicted in Fig. 2A. The area under the curve (AUC) described the overall influx of Ca^{2+} to the cytosol, which can be further rendered by the Ca^{2+} maximum helping as a descriptive factor of the curve development. In addition, the time to reach a plateau was also measured to gain knowledge about the binding duration between the stimulatory molecules and the receptors. Fig. 2B depicts the Ca^{2+}-dependent fluorescent patterns obtained upon incubation of the T cells with different aAPCs. The normalization to the fluorescent signal of resting T cells unveiled the overall difference in Ca2+ influx between activated and non-activated cells. The results illustrate a clear difference between NP-N3 and NP-Mal, where both maleimide particles resulted in a lower curve than azide, leading to lower AUC values (Fig. 2C). More in detail, the AUC values were different depending on the density of functionalizable groups present on the nanoparticles, with low density being slightly smaller compared to their high covered counterpart, which correlates with the theory of more TCR-engagement taking place due to more stimulatory molecules being present. When looking at the maximum fluorescent intensity values achieved (Fig. 2D), similar patterns were observed (NP-N3 high > NP-N3 low > NP-Mal high > NP-Mal low). This pattern was also described by Christo et al where lower Ca^{2+} levels are achieved when using monovalent fab' aCD3 fragments compared to bivalent full antibodies,[46] which can be explained by the binding affinity of full antibodies being reported to be 2–3 higher.[47] In addition, the time to reach Ca2+ max (tmax) also highlights different behavior in the synapsis between the aACPs and the T cells (Fig. 2E). NP-N3 low reached its Ca2+ influx maximum the first, followed by NP-Mal low and NP-N3 high having similar values, and NP-Mal high binding the longest. This indicates a shorter binding of the random immobilized aAPCs compared to the NP-Mal aAPCs, despite the bivalence of the random immobilized aAPCs. We hypothesize a longer binding occur overcoming steric hindrance caused by random immobilized ligands. In conclusion, these results underscore the importance of antibody orientation, density, and valence on nanoparticles in influencing the binding behavior of aAPCs to T cells. While it's important to note that there may not be a statistically significant difference observed, the trends we have identified indicate that antibody exposure does have an impact. These factors should be considered as fundamental parameters in the design of aAPCs.

2.3. Granzyme B analysis validates biological activity of the cell product

After validation of the binding properties, the next step was to

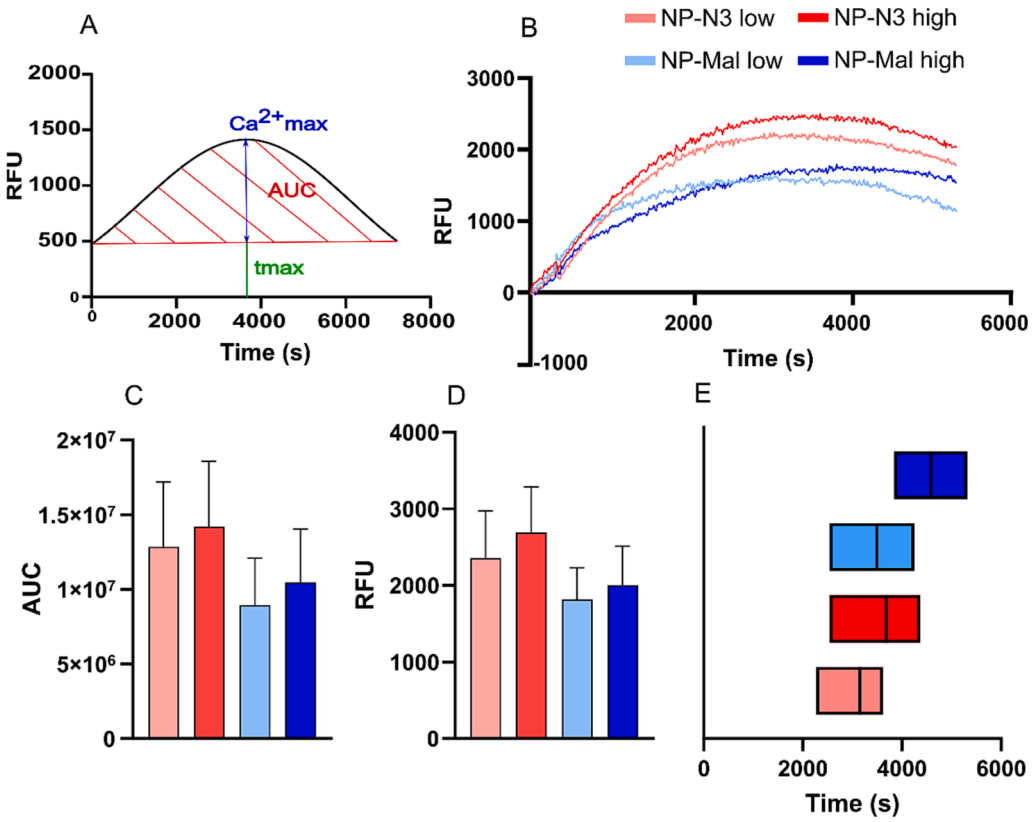

Fig. 2. Azide and Maleimide functionalized nanoparticles show distinct Ca^{2+} responses. (A) Schematic overview on extracted data of Ca^{2+} influx kinetics. In black is a representative curve of the Ca^{2+} levels in the cytosol of T cells measured using Fluo-4AM calcium indicator, green represents the speed at half maximum signal, in blue is the Ca2+ maximum and in red is the area under the curve (AUC). (B) Average Ca^{2+} signal, normalized to resting T cells. T cells were incubated with a final concentration of 0.2 mg/ml nanoparticles. (C) Area under the curve analysis of three independent experiments. (D) Maximum fluorescence signal normalized to resting T cells. (E) Calcium influx tmax values presented as median weighted min–max plots (s). All graphs represent mean ± SE from three independent experiments. (For interpretation of the references to colour in this figure legend, the reader is referred to the web version of this article.)

evaluate the functionality of the T cells upon activation with the aACPs. Granzyme B (GrB) secretion is the state-of-the-art marker to assess the cytotoxicity of the cell product.[48] Analysis of the supernatants of the T cells incubated with the aACPs by ELISA showed a clear increase in GrB levels compared to the untreated control (Fig. 3). Furthermore, both conjugation strategies showed a trend of increased GrB secretion proportional to their antibody coverage. This corroborates the activation potential of our chosen conjugation strategies.

2.4. *The effective ligand density window for T cell expansion is influenced by the antibody orientation*

In the context of T cell activation, expansion numbers play a key role to produce sufficient cell product for therapy, as a low dose treatment in most cases range between 0.08–0.81 × 10^9 cells per patient.[49] To evaluate the impact of antibody orientation and density on the expansion of human polyclonal $CD8^+$ T cells, we isolated blood-derived T cells from three different donors. Once isolated, 10^6 T cells/ml were treated with 200 μg/ml aAPCs and the expansion and viability were monitored for 7 days. Untreated (UT) cells were cultured with 10 ng/ml IL-2 without further stimulants. As a control, we have used ImmunoCult according to the manufactures' protocol.[50] Visual examination of the T cell cultures revealed that azide functionalized particles (NP-N3) induced smaller clusters of T cells after 3 days compared to Maleimide particles (NP-Mal) and ImmunoCult, indicating differences in the activation properties of the various aAPCs (Fig. 4A). A previous study has shown that the secondary T cell – T cell synaptic interaction after APC – T cell interaction supports T cell differentiation, underlying our hypothesis.[51] Evaluation of the expansion profile revealed a different pattern between the two orientations. While low surface coverage showed a higher expansion fold compared to high in NP-Mal particles, the opposite was observed between the azide particles (Fig. 4B). In detail, 5 days after activation with the particles, T cells expansion rates were from high to low: NP-Mal low > NP-N3 high > NP-N3 low > NP-Mal high. Of note, NP-N3 low showed lower expansion rates compared to NP-N3 high, indicating a lack of complete activation when using the azide particles with lower antibody coverage. Interestingly, the maleimide system showed the contrary, where NP-Mal high had decreased expansion rates compared to the NP-Mal low. Hickey et al have shown that expansion rates correlate with the concentration of activation signals until they reach a plateau, and then fall again as an indicator of overstimulation, suggesting an optimal ligand density window for T cell activation[52]. The results suggest that the better orientation of the maleimide-coupled antibodies requires a lower amount of antibodies than when having them randomly immobilized on the surface of the particle. Even though bivalent antibodies can crosslink more receptors than monovalent antibodies, controlled immobilization is crucial for the design of improved artificial cell-activating particles to fine-tune the expansion potential of T cells. In addition to T cell proliferation, monitoring the cell viability over time is also important to evaluate the quality of the expanded cell product. Overall, the results indicated a healthy expansion protocol (Fig. 4C). NP-N3 low, NP-N3 high and NP-Mal low showed viability values of around 96 % throughout culturing, while NP-Mal high showed a decrease of viability after 5 days to 89 % suggesting overstimulation of the T cells. This correlates with expansion values, where T cells reduced proliferation rates upon harsh stimulation. After 7 days, the cells recovered back to 96 % viability. We hypothesize that the prolonged binding of NP-Mal high particles with the T cells, as seen by the calcium influx rates (Fig. 2E), may lead cell exhaustion similarly to a chronic antigen exposure that leads to fast exhaustion of the T cell.[53,54] The obtained outcome demonstrates a difference in the T cell activation threshold between the two coupling methods. Specifically, well-oriented aAPCs exhibit an effective ligand density window at a lower threshold compared to randomly oriented aAPCs.

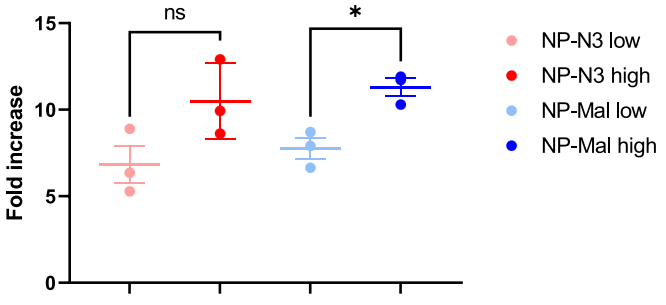

Fig. 3. Nanoparticles increase cytotoxicity of T cells proportionally with AB surface coverage: Granzyme B secretion of T cells after being cultured with NPs for 24 h. The results are shown as fold increase compared to non-activated T cells. Data is shown as mean with SD (n = 3). (P values for ns = 0.0933 and * = 0.0109).

3. T cell marker expression analysis reveals differences in the aAPC design on a molecular level

Another important aspect of T cell expansion is the phenotype of the final product[55]. T cell marker analysis provide great insights into the activation status of the cell prior to adoptive transfer. Hereby, we have used flow cytometry to investigate the effect of the nanoparticles on the T cell marker expression through analyzing levels of CD45RA, CD45RO, CCR7 and CD62L. CD45RA, an early activation marker, which is expressed mostly on naïve cells, fades upon antigen encounter and reoccurs in a late activation state, providing insight into the overall differentiation profile of the T cell[56]. NP-Mal high yielded the highest percentage of CD45RA+ but displayed lower MFI values, indicating a generally low expression of this marker in this population and pointing to a more differentiated phenotype (Fig. 5A). NP-N3 low tends to have a lower percentage of CD45RA+ but a higher MFI value suggesting a slightly increased percentage of non-activated T cells while all other particle systems induced similar CD45RA+ percentages with slightly lower MFI values, showing an overall activated status (Supplementary 3A). Additionally, a pronounced difference is observed between the regioselective- and randomly conjugated aAPCs. The latter showed no significant variation in their marker expression despite variations in ligand density as compared to well-oriented aAPCs, thereby emphasizing the importance of the conjugation scheme. As a second marker we investigated the isoform CD45RO+, mainly expressed on central memory and effector memory cells, thus antigen-experienced cells.[57,58] Here, NP-N3 low resulted in the lowest values underlining our hypothesis of an increased proportion of non-activated T cells compared to the other particles (Fig. 5B). As a third marker, we have chosen CCR7 as it plays an important role in defining subsets of CD8+ T cells, mainly exposed on memory cells, thus being present T cells with a robust proliferative capacity and antigen experience[59]. What stands out in our results is a significant and noteworthy difference between the NP-Mal high and NP-Mal low (Fig. 5C). Here, NP-Mal low had a lower percentage of CCR7+ cells suggesting a more younger phenotype compared to the NP-Mal high population, which displayed a high proportion of CCR7 +. Again both randomly conjugated aAPCs exhibited no difference despite their ligand density, underlining the impact of the surface chemistry used. In regards to their potential therapeutic outcome, we evaluated the homing molecule L-Selecting (CD62L), a marker that is expressed on naïve cells, but also on early T cell phenotypes such as stem cell-like (Tscm) and central memory cells. CD62L appeared to be connected with tumor growth control when being expressed on antigen-experienced T cells[60]. We observed the lowest expression of CD62L on NP-N3 low (52 %) (Fig. 5D). All other particles showed percentages above 60 %, indicating a higher antibody coverage is needed when using a random immobilizing conjugation technique compared to the well-oriented NPs. The final phenotype (Fig. 5E) reveals noteworthy distinctions. Notably, NP-Mal high displays a higher percentage of central

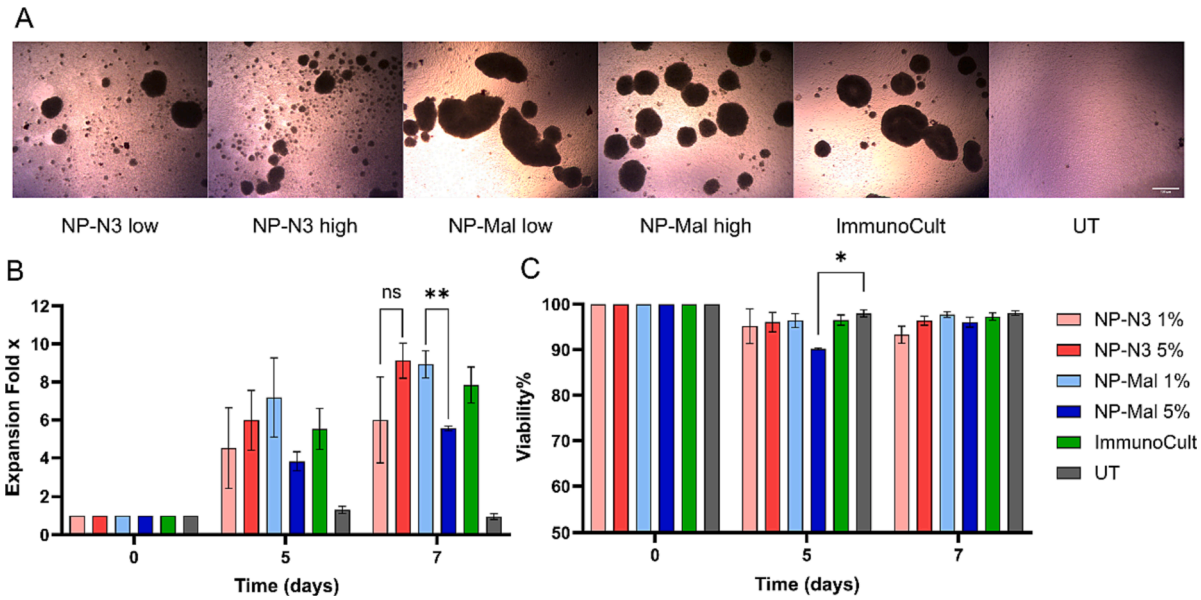

Fig. 4. Random and well oriented conjugated aAPCs show opposite expansion rates concerning their ligand density (A) Light microscope images of cell culture three days after activation with nanoparticles, scale bar represents 100 μm. (B) T cell proliferation after activation was monitored over 7 days. Cells were counted after splitting. (C) Cell viability of the T cells during activation and expansion. Commercial ImmunoCult was used as benchmark control. UT, untreated cells. Error bars represent SEM with n = 3. Scale bar equals 100 μm. P values represent: ns = 0.2688 * =0.0289 **= 0.0100.

memory phenotype compared to the other particles, particularly NP-Mal low. In contrast, both NP-N3 high and low exhibit similar phenotypic percentages, highlighting the differences between the two coupling methods. However, since the development of T cells is a very dynamic process the picture may change overtime. Studies have shown differences in the phenotype of human T cells from patient to patient, which indicates a higher number of donors may be required to account for those inherent donor variations.[53,61] To overcome this, single-cell RNA sequence studies may help to identify specific phenotypic changes in the T cell population, which would be beyond the scope of the present study[62,63]. Nonetheless, the results underline the importance of well-oriented AB for achieving different status of T cell activation by aAPCs.

4. Conclusion

In this work we presented a workflow to evaluate the impact of antibody orientation, density and valence on PLGA nanoparticle model systems for polyclonal $CD8^+$ T cell expansion utilizing two different antibody coupling chemistries. All synthesized particles exhibited comparable sizes and surface charges, maintaining integral colloidal stability both before and after the coupling of aCD3 and aCD28 antibodies. Amine targeting TFP coupling leads to a non-controlled random orientation of the antibody on the surface of nanoparticles, requiring a higher amount of antibodies immobilized to fully activate T cells. On contrary, reduced half-antibodies coupled to maleimide groups allow controlled orientation of the antibody and higher accessibility towards the antigen-binding site, leading to full activation, even at lower antibody densities. Even though maleimide particles contained monovalent half-antibodies, the right orientation showed superior behavior for polyclonal expanding T cells than the random immobilized counterparts. The workflow presented herein describes a set of methods, such as $Ca2^+$ influx, Granzyme B secretion, expansion and viability measurements, and surface marker expression that allow characterization of the chosen parameters on the aAPCs and their impact on T cell interaction and further activation. We could show that differences in the density influence intracellular Calcium levels that further lead to deviations in downstream processes such as Granzyme B secretion, underlining the robustness of both coupling techniques. Moreover, we clearly showed by analyzing expansion, viability and that both coupling techniques differ in their effective window activating and expanding T cells, with regio-selective coupled aAPCs at a lower threshold in contrast to randomly-oriented aAPCs. Further, well-oriented aAPCs had a direct impact on the surface marker expression, depending on their ligand density, thereby emphasizing the criticality of the conjugation scheme when designing aAPCs. Nevertheless, while other expansion methods employing random conjugation techniques have yielded useful clinical products [9], we anticipate a reduced variance in the final product when the conjugation method results in a precisely defined activation bead. To our knowledge, there is a lack of investigation on the impact of antibody orientation on nanoparticles in regards to T cell activation, making this work of high relevance highlighting the importance of designing ideal nano-sized artificial antigen-presenting cells with fine-tuning properties. These findings can help to develop next-generation activation beads for ex vivo expansion protocols of T cells with tailored properties.

5. Materials and methods

5.1. Reagents and materials

All polymers were obtained from NanoSoft Polymers (USA), DBCO-dPEG®$_{12}$-TFP (Iris Biotech Gmbh, Germany), Poly(vinyl alcohol) Mw 13,000–23,000, 87–89 % hydrolyzed (Sigma-Aldrich, Denmark), Dulbecco's Phosphate Buffered Saline (Sigma-Aldrich, Denmark), InVivoMAb anti-human CD3, Clone UCHT1 (Leu-4) (T3), (Nordic BioSite, Denmark), InVivoMAb anti-human CD2, Clone 9.3 (Nordic BioSite, Denmark), BV480 CD45RABV786 Mouse Anti-Human CD62L, FITC anti-human CD8 Antibody,PE anti-human CD197 (CCR7) Antibody, APC anti-human CD45RO (BD Bioscience, Denmark), Fluo4-AM cell permeant, (Thermo Scientific, Denmark).

5.2. Synthesis of T cell activating aAPCs

Nanoparticles (NPs) were synthesized from a polymer blend of poly-(lactic-co-glycolic acid) (PLGA; 50:50 LA:GA ratio; MW 20,000 Da), poly-(lactic-co-glycolic acid)- methoxy-poly-ethylene-oxide (PLGA-PEG; 50:50 LA:GA ratio; MW PLGA 20,000; MW mPEG 2,000 Da), poly-(lactic-co-glycolic acid)-maleimide-poly-ethylene-oxide (PLGA-PEG;

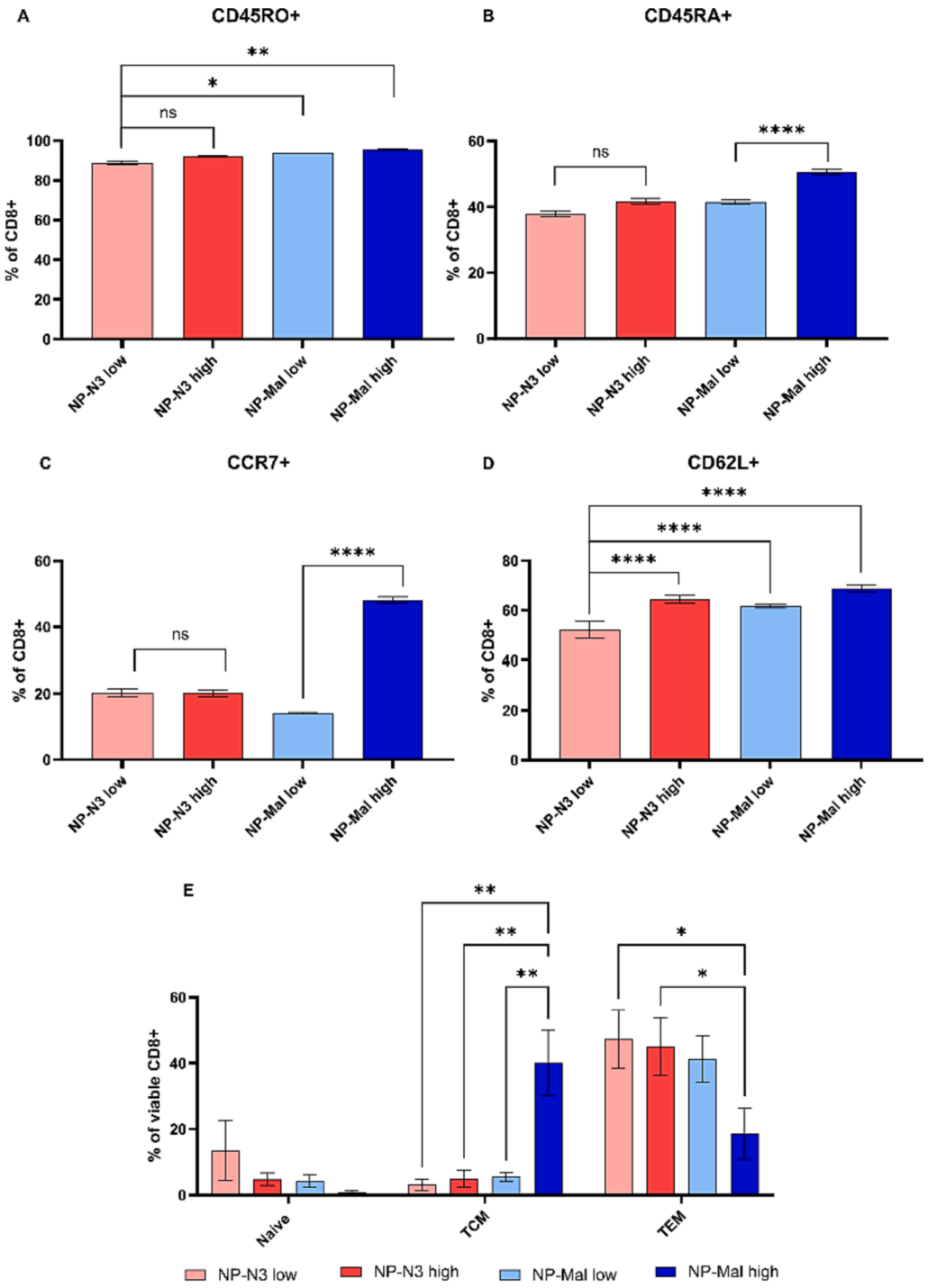

Fig. 5. Flow cytometry analysis of surface markers and aAPC footprint after T cell activation. (A) Percentage CD45RA expression (B) percentage CD45RO expression (C) percentage CCR7 expression (D) percentage CD62L expression in CD8+ T cell population. (E) Phenotype percentage of viable CD8+ T Cells devided in Naïve, central memory (TCM) and effector memory (TEM) cells. All graphs represent three individual experiments using T cells from three different donors. Graphs represent the mean and the standard error of the mean. (ns = 0.1234 *p = 0.0332 **p = 0.0021 ***p = 0.0002 ****p < 0.0001).

50:50 LA:GA ratio; MW PLGA 20,000; MW PEG-Maleimide 2,000 Da), poly-(lactic-co-glycolic acid)-azide-poly-ethylene-oxide (PLGA-PEG; 50:50 LA:GA ratio; MW PLGA 20,000; MW PEG-Azide 2,000 Da). For high covered particles, the blend consisted of 70 wt% PLGA, 25 wt% PLGA-mPEG and 5 wt% PLGA-PEG-Mal or PLGA-PEG-N_3, respectively. For low covered particles, the blend consisted of 70 wt% PLGA, 29 wt% PLGA-mPEG and 1 wt% PLGA-PEG-Mal or PLGA-PEG-N_3, respectively. The nanoparticles were synthesized as previously described by a double emulsion (W/O/W) solvent evaporation method with slight modifications.[64] Briefly, 2 mL PLGA-blend (12.5 mg/mL in Dichloromethane) was added to 250 μL 0.5 M PBS, followed by probe sonication (50 % amplitude, 1 min, 2 sec on/off cycle) (Q700 sonicator with microprobe, Qsonica). The primary emulsion was added to 10 mL 1 % PVA solution and followed by a second probe sonication step (50 % amplitude, 1 min, 2 sec on/off cycle). The resulting double emulsion was left at room temperature for evaporation for 4 h and washed 3 times with milliQ water (3× 1200G, 15 min, 4 °C). To determine the particle concentration a small aliquot was taken and freeze-dried overnight. The

remaining solution was resuspended in a 10 % sucrose solution and lyophilized for further use.

5.3. Preparation of random immobilized activation nanoparticles

Antibodies (antiCD3, Clone UCHT1 (Leu-4)(T3) and antiCD28, clone 9.3 BioXCell) were buffer exchanged to a 0.1 M bicarbonate buffer at pH 8 using spin filtration (10 kDa cutoff polyethersulfone (PES) membrane, Vivaspin 500, Sigma Aldrich, Denmark) two times. The final concentration was measured via UV–Vis spectroscopy using a Nanodrop spectrophotometer (Thermofisher, Denmark) at 280 nm wavelength. The concentration was calculated according to the manufacturer datasheet using a 1.33 absorbance coefficient and set to 2 mg/ml (13.2 μM) in a protein low binding Eppendorf tube. DBCO-dPEG®$_{12}$-TFP ester (Iris Biotech Gmbh, Germany) was dissolved in anhydrous DMSO at a final concentration of 10 mM. To 100 μL of the antibody solution, 1.6 μL DBCO-dPEG®$_{12}$-TFP ester was added and let react for 30 min under shaking conditions at 25 °C. The reaction was quenched with 400 μL TRIS-Buffer (pH 7.2) and unreacted parts were washed out with PBS by spin filtration (Molecular cutoff: 10 kDa). The amount of DBCO per Antibody was determined by measuring UV–Vis at 280 nm and 310 nm, respectively, and calculated using the following equations:

a. $A_{IgG} = A_{280}\text{-}(A_{310} * f)$; f = correction factor DBCO at 280 nm = 1.089.
b. $C_{IgG} = A_{280}/(204{,}000\ M^{-1}\ cm^{-1} * 0.1\ cm)$.
c. $C_{DBCO} = A_{310}/(12{,}000\ M^{-1}\ cm^{-1} * 0.1\ cm)$.
d. Ratio = C_{DBCO}/C_{IgG}.

Hereby, equation (a.) describes the concentration of the antibody in the presence of DBCO using a correction factor of 1.089. Equations (b.) and (c.) describe the molar concentration of the antibody and DBCO. The final ratio was determined using equation (d.). In total, 20 μg of each antibody were added to the particles at a final concentration of 4 mg/mL and left for reaction overnight at room temperature. PLGA-NPs were then washed three times with sterile 0.1 M PBS and used immediately for cell experiments.

5.4. Preparation of coordinated immobilized activation nanoparticles

Antibodies (antiCD3 and antiCD28) were buffer exchanged to a borate buffered saline (BBS) solution (50 mM sodium borate, 50 mM NaCl and 5 mM ethylenediaminetetraacetic acid (EDTA), at pH 8.5.) via spin filtration (10 kDa cutoff, PES membrane) two times. The final antibody concentration was determined as described above and set to 13.2 μM. Tris(2-carboxyethyl)phosphine hydrochloride (TCEP-HCl) was dissolved in BBS at a final concentration of 10 mM. To the antiCD3 and antiCD28 solution, 6 and 8 M equivalents of TCEP were added respectively and left for reacting for 30 min at 37 °C under mild agitation. The reduced antibodies were washed by spin filtration with 0.1 M PBS containing 5 mM EDTA and the concentration was determined at 280 nm UV–VIS. Lyophilized particles were resuspended in 0.1 M PBS containing 5 mM EDTA and washed twice to remove the sucrose. 15 μg of each antibody were given to the particles at a final concentration of 2 mg/mL and left for reaction overnight at 5 °C under shaking conditions. The nanoparticles were then washed three times with sterile PBS and used immediately for cell experiments.

5.5. Physicochemical analysis of the particles

Hydrodynamic diameter, polydispersity and Zeta potential were measured by dynamic light scattering (DLS) using a Nano ZS from Malvern Instruments (Malvern, Worcestershire, UK). Briefly, 50 mg PLGA-NPs were diluted in 1 mL milliQ water and measured in the Nano ZS. Results obtained were the average from 3 runs of 12 cycles. For morphological analysis, the particles were analyzed using scanning electron microscopy (SEM). Sample solutions (50 μL) were deposited onto clean silicon wafer pieces and allowed to adsorb for 1 min before excess solution was wicked away using filter paper. Samples were then left to fully dry, sputter coated with ~ 5 nm Au layer, and imaged using a Quanta FEG 200 SEM operated at high vacuum with an accelerating voltage of 5 kV.

5.6. Antibody coverage of the nanoparticles

Antibodies were prior reaction fluorophore-labeled using the Lightning Link conjugation kit (fast) from Abcam according to the manufacturer's protocol. Briefly, antibodies for DBCO copper-free click conjugation were labeled with AF488 and AF647. Antibodies for maleimide reactions were labeled with AF488 and Atto 635. The reaction for antibody conjugation was carried out as described above. Fluorescence intensities of the thoroughly washed particles and the supernatants were measured using a Tecan plate reader (Switzerland). Concentrations were extrapolated from a standard curve made with known amounts of the labeled antibodies.

5.7. T cell isolation, culture and expansion

CD8+ T cells were isolated from the blood of healthy volunteers following the ethical guidelines of Danish authorities and according to DTU guidelines that includes protection of the donor and the researchers using the EasySep™ Human CD8+ T cell isolation kit from Stemcell, according to the manufacturer protocol. After that, T cells were resuspended and cultured at a concentration of 10^6 cells/mL in RPMI containing 10 % FBS, 1 % PS, 1 % nonessential amino acids and 10 ng/mL human Interleukin-2. Cells (200 μL) were plated in flat-bottom 96-well plates and incubated at 37 °C and 5 % CO_2. For activation experiments, particles were added at a final concentration of 0.2 mg/mL. As controls, untreated cells were not exposed to antiCD3 and antiCD28 antibodies, and activated cells received ImmunoCult™ Human CD3/CD28 T cell activator dendrimers according to the manufacturer protocol. Particles were incubated for three days with the cells until they got transferred to a 48-well plate with double the volume of media added. After five days the cells were then transferred to a 24-well plate using again double the volume of media. After five and seven days a small aliquot was taken for counting the cells and measuring viability using a NucleoCounter NC-200 (ChemoMetec, Denmark).

5.8. Ca2+ influx measurements

Freshly isolated naïve T cells were stained with Fluro-4am, a fluorescent Ca2+ indicator, according to the manufacturer's protocol. Briefly, 10^6 cells/mL were stained with 3 μM Fluoro-4AM for 30 min at 37 °C and 5 % CO_2. Afterwards cells were washed and resuspended in full media to cleave of any remaining esters. 150 μL of cells were then transferred to a black flat-bottom 96-well plate and fluorescence intensity was measured for five minutes in 15-second intervals to assess the background level of Ca2+. Then 50 μL of particle suspension was given to the cells to reach a final concentration of 0.2 mg/ml. Fluorescence intensities (485 nm/ 535 nm with 20 nm bandwidth) were measured immediately after the addition of the particles for three hours every 15 s. The measured data was then normalized against the control that has not been activated and analyzed as the mean of three separate experiments.

5.9. Granzyme B detection

Freshly isolated naïve T cells were seeded in full media in a 96-well plate at a concentration of 10^6 cells/mL. Then particles were added to a final concentration of 0.2 mg/ml and the culture was kept for 24 h. After that T cells were spun down at 400 G for 3 min and the supernatants were collected. The supernatants were then analyzed using a Human Granzyme B DuoSet ELISA (R&D Systems, UK) kit according to the

manufacturers' protocol.

5.10. Flow cytometry analysis of expanded T cells

Seven days after activation, T cells were counted and set to a final concentration of 10^6 cells/mL. From that cell suspension, 100 μL were FC blocked and stained for the markers CD8 (antiCD8-FITC), CD45RA (antiCD45RA-BV480), CD45RO (antiCD45RO-APC), CCR7 (antiCCR7-PE) and CD62L (anti-CD62L-BV786) for 30 min on ice with various concentration according to internal dilution series. eBioscience Fixable Viability Dye eFluor780 was used to assess viability. The T cells were washed and fluorescence signals were measured using a BD-Fortessa flow cytometer collecting 30,000 events and analyzed using Flow-Jo software V.10.

CRediT authorship contribution statement

Sven Weller: Writing – review & editing, Writing – original draft, Project administration, Methodology, Investigation, Formal analysis, Data curation, Conceptualization. **Xin Li:** Investigation, Formal analysis, Data curation. **Lars R. Petersen:** Writing – review & editing, Supervision, Conceptualization. **Paul Kempen:** Formal analysis, Data curation. **Gael Clergeaud:** Writing – review & editing, Validation, Supervision, Formal analysis, Conceptualization. **Thomas L. Andresen:** Writing – review & editing, Supervision, Project administration, Funding acquisition, Conceptualization.

Declaration of competing interest

The authors declare that they have no known competing financial interests or personal relationships that could have appeared to influence the work reported in this paper.

Data availability

Data will be made available on request.

Acknowledgments

Schemes were created by BioRender.com. We would like to thank Fredrik Melander for fruitful discussions and input on the manuscript. This work was supported by grant no. 5164-00010B from Innovation Fund Denmark and the Novo Nordisk foundation Grant No. NNF16OC0022166.

Appendix A. Supplementary material

Supplementary data to this article can be found online at https://doi.org/10.1016/j.intimp.2024.111643.

References

[1] S.R. Riddell, P.D. Greenberg, Principles for adoptive t cell therapy of human viral diseases, Annu. Rev. Immunol. 13 (1995) 545–586, https://doi.org/10.1146/annurev.iy.13.040195.002553.
[2] C.J.M. Melief, W.M. Kast, T-Cell immunotherapy of tumors by adoptive transfer of cytotoxic T lymphocytes and by vaccination with minimal essential epitopes, Immunol. Rev. 145 (1995) 167–177, https://doi.org/10.1111/J.1600-065X.1995.TB00081.X.
[3] C.M. Mousset, W. Hobo, R. Woestenenk, F. Preijers, H. Dolstra, A.B. van der Waart, Comprehensive phenotyping of T cells using flow cytometry, Cytom. Part A 95 (2019) 647–654, https://doi.org/10.1002/cyto.a.23724.
[4] C. Wang, M. Singer, A.C. Anderson, Molecular dissection of CD8+ T-Cell dysfunction, Trends Immunol. 38 (2017) 567–576, https://doi.org/10.1016/J.IT.2017.05.008.
[5] C.S. Hinrichs, Z.A. Borman, L. Gattinoni, Z. Yu, W.R. Burns, J. Huang, C. A. Klebanoff, L.A. Johnson, S.P. Kerkar, S. Yang, P. Muranski, D.C. Palmer, C. D. Scott, R.A. Morgan, P.F. Robbins, S.A. Rosenberg, N.P. Restifo, Human effector CD8+ T cells derived from naive rather than memory subsets possess superior traits for adoptive immunotherapy, Blood. 117 (2011) 808–814, https://doi.org/10.1182/blood-2010-05-286286.
[6] C.S. Hinrichs, Z.A. Borman, L. Cassard, L. Gattinoni, R. Spolski, Y. Zhiya, L. Sanchez-Perez, P. Muranski, S.J. Kern, C. Logun, D.C. Palmer, J. Yun, R.N. Reger, W.J. Leonard, R.L. Danner, S.A. Rosenberg, N.P. Restifo, Adoptively transferred effector cells derived from naïve rather than central memory CD8+ T cells mediate superior antitumor immunity, Proc. Natl. Acad. Sci. u. s. a. 106 (2009) 17469–17474, https://doi.org/10.1073/pnas.0907448106.
[7] J.G. Crompton, M. Sukumar, N.P. Restifo, Uncoupling T-cell expansion from effector differentiation in cell-based immunotherapy, Immunol. Rev. 257 (2014) 264–276, https://doi.org/10.1111/imr.12135.
[8] E.R. Steenblock, T.M. Fahmy, A comprehensive platform for Ex Vivo T-cell expansion based on biodegradable polymeric artificial antigen-presenting cells, Mol. Ther. 16 (2008) 765–772, https://doi.org/10.1038/MT.2008.11.
[9] J. Ichikawa, T. Yoshida, A. Isser, A.S. Laino, M. Vassallo, D. Woods, S. Kim, M. Oelke, K. Jones, J.P. Schneck, J.S. Weber, Rapid Expansion of highly functional antigen-specific T cells from patients with melanoma by nanoscale artificial antigen-presenting cells, Clin. Cancer Res. 26 (2020) 3384–3396, https://doi.org/10.1158/1078-0432.CCR-19-3487.
[10] M.M. Suhoski, T.N. Golovina, N.A. Aqui, V.C. Tai, A. Varela-Rohena, M.C. Milone, R.G. Carroll, J.L. Riley, C.H. June, Engineering artificial antigen-presenting cells to express a diverse array of Co-stimulatory molecules, Mol. Ther. 15 (2007) 981–988, https://doi.org/10.1038/MT.SJ.6300134.
[11] Q. Zhang, W. Wei, P. Wang, L. Zuo, F. Li, J. Xu, X. Xi, X. Gao, G. Ma, H.-Y. Xie, Biomimetic magnetosomes as versatile artificial antigen-presenting cells to potentiate T-cell-based anticancer therapy, ACS Nano. 11 (2017) 10724–10732, https://doi.org/10.1021/acsnano.7b04955.
[12] B. Prakken, M. Wauben, D. Genini, R. Samodal, J. Barnett, A. Mendivil, L. Leoni, S. Albani, Artificial antigen-presenting cells as a tool to exploit the immune 'synapse', Nat. Med. 6 (2000) 1406–1410, https://doi.org/10.1038/82231.
[13] S. Mandal, Z.H. Eksteen-Akeroyd, M.J. Jacobs, R. Hammink, M. Koepf, A.J. A. Lambeck, J.C.M. van Hest, C.J. Wilson, K. Blank, C.G. Figdor, A.E. Rowan, Therapeutic nanoworms: towards novel synthetic dendritic cells for immunotherapy, Chem. Sci. 4 (2013) 4168, https://doi.org/10.1039/c3sc51399h.
[14] K. Lee, Y. Yu, Janus nanoparticles for T cell activation: clustering ligands to enhance stimulation, J. Mater. Chem. b. 5 (2017) 4410–4415, https://doi.org/10.1039/C7TB00150A.
[15] S. Song, X. Jin, L. Zhang, C. Zhao, Y. Ding, Q. Ang, O. Khaidav, C. Shen, PEGylated and CD47-conjugated nanoellipsoidal artificial antigen-presenting cells minimize phagocytosis and augment anti-tumor T-cell responses , Int. J. Nanomedicine. 14 (2019) 2465–2483, https://doi.org/10.2147/IJN.S195828.
[16] J.C. Sunshine, K. Perica, J.P. Schneck, J.J. Green, Particle shape dependence of CD8+ T cell activation by artificial antigen presenting cells, Biomaterials. 35 (2014) 269–277, https://doi.org/10.1016/j.biomaterials.2013.09.050.
[17] X. Lu, X. Jiang, R. Liu, H. Zhao, Z. Liang, Adoptive transfer of pTRP2-specific CTLs expanding by bead-based artificial antigen-presenting cells mediates anti-melanoma response, Cancer Lett. 271 (2008) 129–139, https://doi.org/10.1016/j.canlet.2008.05.049.
[18] J.W. Hickey, F.P. Vicente, G.P. Howard, H.-Q. Mao, J.P. Schneck, Biologically inspired design of nanoparticle artificial antigen-presenting cells for immunomodulation, Nano Lett. 17 (2017) 7045–7054, https://doi.org/10.1021/acs.nanolett.7b03734.
[19] A.C. Wauters, J.F. Scheerstra, I.G. Vermeijlen, R. Hammink, M. Schluck, L. Woythe, H. Wu, L. Albertazzi, C.G. Figdor, J. Tel, L.K.E.A. Abdelmohsen, J.C.M. van Hest, Artificial antigen-presenting cell topology dictates T cell activation, ACS Nano. 16 (2022) 15072–15085, https://doi.org/10.1021/acsnano.2c06211.
[20] S. Ghaffari, M. Torabi-Rahvar, S. Aghayan, Z. Jabbarpour, K. Moradzadeh, A. Omidkhoda, N. Ahmadbeigi, Optimizing interleukin-2 concentration, seeding density and bead-to-cell ratio of T-cell expansion for adoptive immunotherapy, BMC Immunol. 22 (2021) 43, https://doi.org/10.1186/s12865-021-00435-7.
[21] J. Matic, J. Deeg, A. Scheffold, I. Goldstein, J.P. Spatz, Fine tuning and efficient T cell activation with stimulatory aCD3 nanoarrays, Nano Lett. 13 (2013) 5090–5097, https://doi.org/10.1021/nl4022623.
[22] N. Eivazi, R. Rahmani, M. Paknejad, Specific cellular internalization and pH-responsive behavior of doxorubicin loaded PLGA-PEG nanoparticles targeted with anti EGFRvIII antibody, Life Sci. 261 (2020) 118361, https://doi.org/10.1016/j.lfs.2020.118361.
[23] J. Patel, J. Amrutiya, P. Bhatt, A. Javia, M. Jain, A. Misra, Targeted delivery of monoclonal antibody conjugated docetaxel loaded PLGA nanoparticles into EGFR overexpressed lung tumour cells, J. Microencapsul. 35 (2018) 204–217, https://doi.org/10.1080/02652048.2018.1453560.
[24] V. Stanković, S. Đurđić, M. Ognjanović, B. Antić, K. Kalcher, J. Mutić, D. M. Stanković, Anti-human albumin monoclonal antibody immobilized on EDC-NHS functionalized carboxylic graphene/AuNPs composite as promising electrochemical HSA immunosensor, J. Electroanal. Chem. 860 (2020) 113928, https://doi.org/10.1016/j.jelechem.2020.113928.
[25] A.K. Trilling, J. Beekwilder, H. Zuilhof, Antibody orientation on biosensor surfaces: a minireview, Analyst. 138 (2013) 1619–1627, https://doi.org/10.1039/C2AN36787D.
[26] J.A. Ho, W.-L. Hsu, W.-C. Liao, J.-K. Chiu, M.-L. Chen, H.-C. Chang, C.-C. Li, Ultrasensitive electrochemical detection of biotin using electrically addressable site-oriented antibody immobilization approach via aminophenyl boronic acid, Biosens. Bioelectron. 26 (2010) 1021–1027, https://doi.org/10.1016/j.bios.2010.08.048.
[27] E.J. Franco, H. Hofstetter, O. Hofstetter, A comparative evaluation of random and site-specific immobilization techniques for the preparation of antibody-based

chiral stationary phases, J. Sep. Sci. 29 (2006) 1458–1469, https://doi.org/10.1002/jssc.200600062.
[28] H.Y. Song, X. Zhou, J. Hobley, X. Su, Comparative Study of Random and Oriented Antibody Immobilization as Measured by Dual Polarization Interferometry and Surface Plasmon Resonance Spectroscopy, Langmuir. 28 (2012) 997–1004, https://doi.org/10.1021/la202734f.
[29] N.J. Alves, T. Kiziltepe, B. Bilgicer, Oriented surface immobilization of antibodies at the conserved nucleotide binding site for enhanced antigen detection, Langmuir. 28 (2012) 9640–9648, https://doi.org/10.1021/LA301887S.
[30] B.N. Lourenço, R.F. Pereira, C.C. Barrias, C. Fischbach, C. Oliveira, P.L. Granja, Engineering Modular Half-Antibody Conjugated Nanoparticles for Targeting CD44v6-Expressing Cancer Cells, Nanomater. 2021, Vol. 11, Page 295. 11 (2021) 295. https://doi.org/10.3390/NANO11020295.
[31] B. Anand, Q. Wu, M. Nakhaei-Nejad, G. Karthivashan, L. Dorosh, S. Amidian, A. Dahal, X. Li, M. Stepanova, H. Wille, F. Giuliani, S. Kar, Significance of native PLGA nanoparticles in the treatment of Alzheimer's disease pathology, Bioact. Mater. 17 (2022) 506–525, https://doi.org/10.1016/j.bioactmat.2022.05.030.
[32] G.T. Hermanson, Bioconjugate Techniques: Third Edition, Bioconjugate Tech. Third Ed. (2013) 275.
[33] A.J. Sivaram, A. Wardiana, C.B. Howard, S.M. Mahler, K.J. Thurecht, Recent advances in the generation of antibody-nanomaterial conjugates, Adv. Healthc. Mater. 7 (2018) 1700607, https://doi.org/10.1002/adhm.201700607.
[34] M. Brückner, J. Simon, K. Landfester, V. Mailänder, The conjugation strategy affects antibody orientation and targeting properties of nanocarriers, Nanoscale. 13 (2021) 9816–9824, https://doi.org/10.1039/D0NR08191D.
[35] B.F. Lillemeier, M.A. Mörtelmaier, M.B. Forstner, J.B. Huppa, J.T. Groves, M. M. Davis, TCR and Lat are expressed on separate protein islands on T cell membranes and concatenate during activation, Nat. Immunol. 11 (2010) 90–96, https://doi.org/10.1038/ni.1832.
[36] X.-R. Shao, X.-Q. Wei, X. Song, L.-Y. Hao, X.-X. Cai, Z.-R. Zhang, Q. Peng, Y.-F. Lin, Independent effect of polymeric nanoparticle zeta potential/surface charge, on their cytotoxicity and affinity to cells, Cell Prolif. 48 (2015) 465–474, https://doi.org/10.1111/CPR.12192.
[37] G.J. Pillai, M.M. Greeshma, D. Menon, Impact of poly(lactic-co-glycolic acid) nanoparticle surface charge on protein, cellular and haematological interactions, Colloids Surfaces B Biointerfaces. 136 (2015) 1058–1066, https://doi.org/10.1016/J.COLSURFB.2015.10.047.
[38] Å. Danielsson, A. Ljunglöf, H. Lindblom, One-step purification of monoclonal IgG antibodies from mouse ascites, J. Immunol. Methods. 115 (1988) 79–88, https://doi.org/10.1016/0022-1759(88)90312-2.
[39] I. Laux, A. Khoshnan, C. Tindell, D. Bae, X. Zhu, C.H. June, R.B. Effros, A. Nel, Response differences between Human CD4+ and CD8+ T-Cells during CD28 costimulation: implications for immune cell-based therapies and studies related to the expansion of double-positive T-cells during aging, Clin. Immunol. 96 (2000) 187–197, https://doi.org/10.1006/clim.2000.4902.
[40] I.D. Dimitriou, K. Lee, I. Akpan, E.F. Lind, V.A. Barr, P.S. Ohashi, L.E. Samelson, R. Rottapel, Timed regulation of 3BP2 induction is critical for sustaining CD8+ T cell expansion and differentiation, Cell Rep. 24 (2018) 1123–1135, https://doi.org/10.1016/j.celrep.2018.06.075.
[41] W. Zhang, C.L. Sommers, D.N. Burshtyn, C.C. Stebbins, J.B. DeJarnette, R.P. Trible, A. Grinberg, H.C. Tsay, H.M. Jacobs, C.M. Kessler, E.O. Long, P.E. Love, L. E. Samelson, Essential role of LAT in T cell development, Immunity. 10 (1999) 323–332, https://doi.org/10.1016/S1074-7613(00)80032-1.
[42] K. Choudhuri, M.L. Dustin, Signaling microdomains in T cells, FEBS Lett. 584 (2010) 4823–4831, https://doi.org/10.1016/j.febslet.2010.10.015.
[43] C. Wülfing, J.D. Rabinowitz, C. Beeson, M.D. Sjaastad, H.M. McConnell, M. M. Davis, Kinetics and extent of T cell activation as measured with the calcium signal, J. Exp. Med. 185 (1997) 1815–1825, https://doi.org/10.1084/jem.185.10.1815.
[44] N. Joseph, B. Reicher, M. Barda-Saad, The calcium feedback loop and T cell activation: how cytoskeleton networks control intracellular calcium flux, Biochim. Biophys. Acta - Biomembr. 2014 (1838) 557–568, https://doi.org/10.1016/J.BBAMEM.2013.07.009.
[45] J.-L. Chen, A.J. Morgan, G. Stewart-Jones, D. Shepherd, G. Bossi, L. Wooldridge, S. L. Hutchinson, A.K. Sewell, G.M. Griffiths, P.A. van der Merwe, E.Y. Jones, A. Galione, V. Cerundolo, Ca 2+ release from the endoplasmic reticulum of NY-ESO-1–specific T cells is modulated by the affinity of TCR and by the use of the CD8 coreceptor, J. Immunol. 184 (2010) 1829–1839, https://doi.org/10.4049/jimmunol.0902103.
[46] S.N. Christo, K.R. Diener, R.E. Nordon, M.P. Brown, H.J. Griesser, K. Vasilev, F. C. Christo, J.D. Hayball, Scrutinizing calcium flux oscillations in T lymphocytes to deduce the strength of stimulus, Sci. Rep. 5 (2015) 7760, https://doi.org/10.1038/srep07760.
[47] L. Kjer-Nielsen, M.A. Dunstone, L. Kostenko, L.K. Ely, T. Beddoe, N.A. Mifsud, A. W. Purcell, A.G. Brooks, J. McCluskey, J. Rossjohn, Crystal structure of the human T cell receptor CD3εγ heterodimer complexed to the therapeutic mAb OKT3, Proc. Natl. Acad. Sci. 101 (2004) 7675–7680, https://doi.org/10.1073/PNAS.0402295101.
[48] S. Mellor-Heineke, J. Villanueva, M.B. Jordan, R. Marsh, K. Zhang, J.J. Bleesing, A. H. Filipovich, K.A. Risma, Elevated granzyme B in cytotoxic lymphocytes is a signature of immune activation in hemophagocytic lymphohistiocytosis, Front. Immunol. 4 (2013) 72, https://doi.org/10.3389/fimmu.2013.00072.
[49] M. Wermke, A.-M. Tsimberidou, A. Mohamed, A. Mayer-Mokler, A. Satelli, C. Reinhardt, D. Araujo, D. Maurer, G.J. Blumenschein, H. Singh, J. Luke, K. Guenther, M. Kalra, M. Chatterjee, N. Hilf, R. Mendrzyk, S. Walter, S. Eck, T. A. Holderried, T. Weinschenk, V. Morris, W. Alsdorf, C.M. Britten, 959 Safety and anti-tumor activity of TCR-engineered autologous, PRAME-directed T cells across multiple advanced solid cancers at low doses – clinical update on the ACTengine® IMA203 trial, J. Immunother. Cancer. 9 (2021) A1009–A, https://doi.org/10.1136/jitc-2021-SITC2021.959.
[50] ImmunoCult™ Human CD3/CD28 T Cell Activator Human T cell activation and expansion reagent, (2021).
[51] A. Gérard, O. Khan, P. Beemiller, E. Oswald, J. Hu, M. Matloubian, M.F. Krummel, Secondary T cell–T cell synaptic interactions drive the differentiation of protective CD8+ T cells, Nat. Immunol. 14 (2013) 356–363, https://doi.org/10.1038/ni.2547.
[52] J.W. Hickey, Y. Dong, J.W. Chung, S.F. Salathe, H.C. Pruitt, X. Li, C. Chang, A. K. Fraser, C.A. Bessell, A.J. Ewald, S. Gerecht, H.Q. Mao, J.P. Schneck, Engineering an artificial T-cell stimulating matrix for immunotherapy, Adv. Mater. 31 (2019), https://doi.org/10.1002/adma.201807359.
[53] G.J. Martinez, R.M. Pereira, T. Äijö, E.Y. Kim, F. Marangoni, M.E. Pipkin, S. Togher, V. Heissmeyer, Y.C. Zhang, S. Crotty, E.D. Lamperti, K.M. Ansel, T. R. Mempel, H. Lähdesmäki, P.G. Hogan, A. Rao, The transcription factor NFAT promotes exhaustion of activated CD8 + T cells, Immunity. 42 (2015) 265–278, https://doi.org/10.1016/j.immuni.2015.01.006.
[54] N. Bortoletto, E. Scotet, Y. Myamoto, U. D'Oro, A. Lanzavecchia, Optimizing anti-CD3 affinity for effective T cell targeting against tumor cells, Eur. J. Immunol. 32 (2002) 3102–3107, https://doi.org/10.1002/1521-4141(200211)32:11<3102::AID-IMMU3102>3.0.CO;2-C.
[55] M. Kalos, C.H. June, Adoptive T cell transfer for cancer immunotherapy in the era of synthetic biology, Immunity. 39 (2013) 49–60, https://doi.org/10.1016/j.immuni.2013.07.002.
[56] J. Carrasco, D. Godelaine, A. Van Pel, T. Boon, P. van der Bruggen, CD45RA on human CD8 T cells is sensitive to the time elapsed since the last antigenic stimulation, Blood. 108 (2006) 2897–2905, https://doi.org/10.1182/blood-2005-11-007237.
[57] G. Hu, S. Wang, Tumor-infiltrating CD45RO+ Memory T lymphocytes predict favorable clinical outcome in solid tumors, Sci. Rep. 7 (2017) 10376, https://doi.org/10.1038/s41598-017-11122-2.
[58] J.K. Tietze, D. Angelova, M.V. Heppt, M. Reinholz, W.J. Murphy, M. Spannagl, T. Ruzicka, C. Berking, The proportion of circulating CD45RO + CD8 + memory T cells is correlated with clinical response in melanoma patients treated with ipilimumab, Eur. J. Cancer. 75 (2017) 268–279, https://doi.org/10.1016/j.ejca.2016.12.031.
[59] H. Choi, H. Song, Y.W. Jung, The roles of CCR7 for the homing of memory CD8+ T cells into their survival niches, Immune Netw. 20 (2020) 1–15, https://doi.org/10.4110/in.2020.20.e20.
[60] H.A. Watson, R.R.P. Durairaj, J. Ohme, M. Alatsatianos, H. Almutairi, R. N. Mohammed, M. Vigar, S.G. Reed, S.J. Paisey, C. Marshall, A. Gallimore, A. Ager, L-selectin enhanced T cells improve the efficacy of cancer immunotherapy, Front. Immunol. 10 (2019) 1321, https://doi.org/10.3389/fimmu.2019.01321.
[61] C.A. Fuhrman, W.-I. Yeh, H.R. Seay, P. Saikumar Lakshmi, G. Chopra, L. Zhang, D. J. Perry, S.A. McClymont, M. Yadav, M.-C. Lopez, H. V. Baker, Y. Zhang, Y. Li, M. Whitley, D. von Schack, M.A. Atkinson, J.A. Bluestone, T.M. Brusko, Divergent Phenotypes of Human Regulatory T Cells Expressing the Receptors TIGIT and CD226., J. Immunol. 195 (2015) 145–55. https://doi.org/10.4049/jimmunol.1402381.
[62] M. Andreatta, J. Corria-Osorio, S. Müller, R. Cubas, G. Coukos, S.J. Carmona, Interpretation of T cell states from single-cell transcriptomics data using reference atlases, Nat. Commun. 12 (2021) 2965, https://doi.org/10.1038/s41467-021-23324-4.
[63] P.A. Szabo, H.M. Levitin, M. Miron, M.E. Snyder, T. Senda, J. Yuan, Y.L. Cheng, E. C. Bush, P. Dogra, P. Thapa, D.L. Farber, P.A. Sims, Single-cell transcriptomics of human T cells reveals tissue and activation signatures in health and disease, Nat. Commun. 10 (2019) 4706, https://doi.org/10.1038/s41467-019-12464-3.
[64] M.M.T. Jansman, X. Liu, P. Kempen, G. Clergeaud, T.L. Andresen, P.W. Thulstrup, L. Hosta-Rigau, Hemoglobin-based oxygen carriers incorporating nanozymes for the depletion of reactive oxygen species, ACS Appl. Mater. Interfaces. 12 (2020) 50275–50286, https://doi.org/10.1021/ACSAMI.0C14822.